Topological charge pumping with subwavelength Raman lattices

D. Burba,[1] M. Račiūnas,[1] I. B. Spielman,[2,3,*] and G. Juzeliūnas[1,†]
[1]*Institute of Theoretical Physics and Astronomy, Vilnius University, Saulėtekio 3, LT-10257 Vilnius, Lithuania*
[2]*Joint Quantum Institute, University of Maryland, College Park, Maryland 20742-4111, USA*
[3]*National Institute of Standards and Technology, Gaithersburg, Maryland 20899, USA*

(Received 27 October 2022; accepted 17 January 2023; published 15 February 2023)

Recent experiments demonstrated deeply subwavelength lattices using atoms with N internal states Raman coupled with lasers of wavelength λ. The resulting unit cell was $\lambda/2N$ in extent, an N-fold reduction compared to the usual $\lambda/2$ periodicity of an optical lattice. For resonant Raman coupling, this lattice consists of N independent sinusoidal potentials (with period $\lambda/2$) displaced by $\lambda/2N$ from each other. We show that detuning from Raman resonance induces tunneling between these potentials. Temporally modulating the detuning couples the s and p bands of the potentials, creating a pair of coupled subwavelength Rice-Mele chains. This operates as a topological charge pump that counterintuitively can give half the displacement per pump cycle of each individual Rice-Mele chain separately. We analytically describe this behavior in terms of infinite-system Chern numbers and numerically identify the associated finite-system edge states.

DOI: 10.1103/PhysRevA.107.023309

I. INTRODUCTION

The behavior of one-dimensional (1D) systems is frequently tractable by analytic and numerical methods, often making them ideal prototypes for understanding phenomena that are intractable in higher dimensions. Even noninteracting systems such as those described by the Rice-Mele (RM) model [1] can have nontrivial topology manifesting as protected edge states and quantized topological charge pumping [2]. Here we focus on a recently implemented 1D subwavelength lattice for ultracold atoms built from N Raman-coupled internal states [3,4] and show that adding temporal modulation to the detuning away from Raman resonance can drive transitions between the s- and p-band Wannier states in adjacent lattice sites. In the tight-binding limit, this gives rise to a pair of coupled RM chains with new regimes of topological charge pumping as well as topologically protected edge states.

Conventional optical lattices for ultracold atoms rely on the ac Stark shift to produce potentials proportional to the local optical intensity. As a result, the lattice period cannot be smaller than half the optical wavelength λ without resorting to multiphoton transitions [5,6]. Recently, several techniques have emerged to create lattices with deeply subwavelength structure [3,4,7–10]; each can be understood in terms of "dressed states" created by coupling internal atomic states with one- or two-photon optical or radio-frequency fields [4,11–16]. Here we consider the scheme depicted in Fig. 1(a) relying on sequentially coupling N internal atomic states using two-photon Raman transitions. For resonant couplings of equal strengths, this results in independent adiabatic potentials for each of the N dressed states, displaced by $\lambda/2N$ from each other, as shown by the dashed curves in Fig. 1(b).

This idealized situation is disturbed by unbalancing the coupling strengths, as studied in Ref. [3], or by detuning one or more of the transitions from resonance; the latter situation is plotted in Fig. 1(b). The addition of such perturbations makes evident the $\lambda/(2N)$ periodicity of the adiabatic potential, giving rise to nearest-neighbor (NN) tunneling between sites spaced by a single reduced unit cell. This induced tunneling is generally much stronger than the natural Nth neighbor tunneling of the undisturbed lattice.

Here we focus on the effects of an additional time-modulated detuning which gives rise to an effective tunneling matrix element between s- and p-band Wannier states spaced by $\pm\lambda/(2N)$, leading to a distinctive subwavelength optical lattice. In this lattice the proximity between adjacent sites allows the modulation-induced matrix element to be comparable to or larger than that of the NN tunneling induced by static detuning. Figure 1(c) shows the resulting lattice geometry arising from this description, and Fig. 1(d) unwraps this into a pair of coupled RM chains described by a highly tunable two-leg ladder Hamiltonian with unique topological properties that are the focus of this paper.

We study the topological aspects of this lattice both by considering adiabatic pumping and in terms of edge states. In the former case we show that the added interchain tunneling enables simple pumping trajectories giving per-cycle displacements of zero, one, or two unit cells; by contrast only displacements in units of two sites are possible for the uncoupled RM chains. A displacement by one unit site is also possible in an interacting spinful Rice-Mele chain [17]; however, this falls outside the classification of noninteracting topological systems.

*spielman@nist.gov; http://ultracold.jqi.umd.edu
†gediminas.juzeliunas@tfai.vu.lt

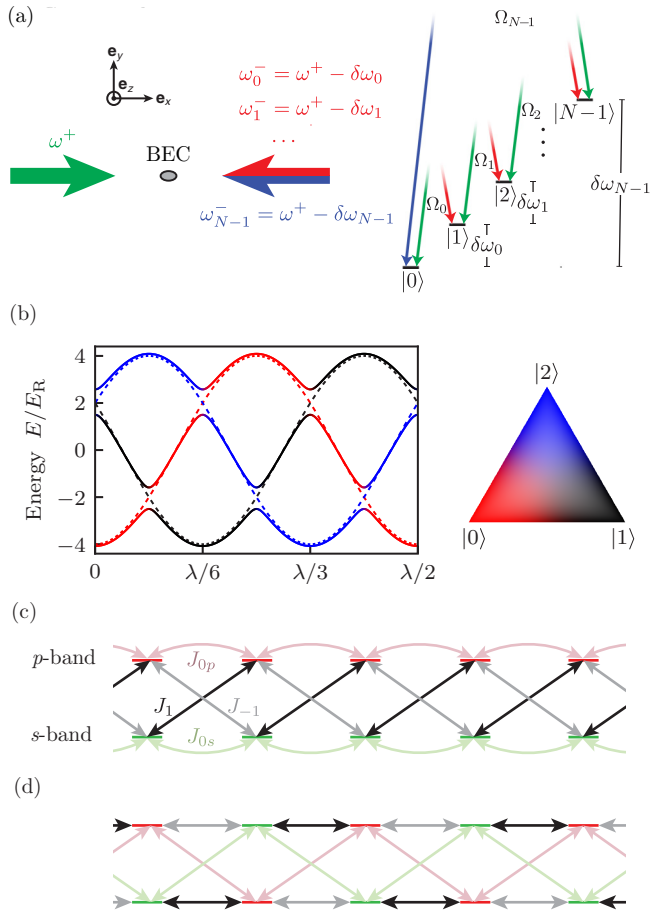

FIG. 1. Lattice concept. (a) Experimental geometry with a single-frequency Raman beam traveling along $\mathbf{e}_x$ and N Raman laser beams sharing the same spatial mode traveling along $-\mathbf{e}_x$. The level diagram for cyclic coupling is depicted on the right. (b) Dressed-state energies for $N = 3$ and $\Omega_0 = \Omega_1 = \Omega_2 = 2E_R$. The dashed curves are computed for zero detuning, whereas the solid ones are calculated for a detuning described by Eq. (17) with $l = 1$ and $\delta = 0.5E_R$. All curves are colored according to the ternary plot on the right, marking the occupation probabilities in the three dressed states (not the bare internal atomic states) obtained by diagonalizing Eq. (16). (c) Tight-binding model. Resonant driving gives nearest-neighbor coupling $J_{\pm 1}$ between the s and p bands. Coupling within bands is induced by a static detuning with matrix elements J_{0s} and J_{0p}. (d) The same lattice unraveled into coupled RM chains. The red and green horizontal bars in (c) and (d) represent atomic positions in the lattice.

This paper is organized as follows. In Sec. II we formally derive the subwavelength Hamiltonian described above. Section III focuses on the subwavelength symmetry operations and solves the resulting band-structure problem. In Sec. IV we obtain a tight-binding description of this lattice in terms of localized s- and p-band Wannier orbitals. The band-changing tunneling induced by time-dependent detuning is derived in Sec. V. Section VI discusses the regimes of topological pumping in the ladder. The regimes of topological edge states are discussed in Sec. VII. Finally, in Sec. VIII we expound on the implications of this work and conclude.

II. HAMILTONIAN

A. Physical geometry

As illustrated in Fig. 1(a), we consider an ensemble of ultracold atoms with N internal atomic ground or metastable states $|j\rangle$, with $j = 0, 1, \ldots, N-1$. These states have nominal energies $\hbar\omega_j$, giving frequency differences $\delta\omega_j = \omega_{j+1} - \omega_j$, where here and below we adopt a periodic labeling scheme for which the labels j and $j+N$ are equivalent; for example, this implies $|j\rangle = |j+N\rangle$ and $\omega_j = \omega_{j+N}$. Notice that for the specific energies depicted in Fig. 1(a), the state vector $|N-1\rangle$ has the largest energy, and $|0\rangle$ has the smallest energy, making their frequency difference $\delta\omega_{N-1} = \omega_0 - \omega_{N-1}$ negative.

The atoms are illuminated by the pair of counterpropagating laser beams depicted in Fig. 1(a) with wavelength λ, defining the single-photon recoil momentum $\hbar k_R = 2\pi\hbar/\lambda$ and energy $E_R = \hbar^2 k_R^2/2m$ for atoms of mass m. The right-going beam (green arrow) has angular frequency ω^+, while the left-going beam (red-blue arrow) has angular frequencies $\omega_j^- = \omega_+ - \delta\omega_j$. These lasers drive two-photon Raman transitions that cyclically couple the internal atomic states; each transition from $|j+1\rangle$ to $|j\rangle$ is characterized by an independent coupling strength Ω_j. The overall transition amplitude $-\Omega_j e^{-i2k_R x}$ includes a phase factor accounting for the two-photon recoil momentum $2\hbar k_R$ imparted by the counterpropagating lasers. The resulting light-matter interaction is described by

$$\hat{V}(x) = -\sum_{j=0}^{N-1} \Omega_j e^{-i2k_R x} |j\rangle\langle j+1| + \text{H.c.}, \tag{1}$$

where the hat signifies an operator that acts on the internal atomic states and we leave implicit the operator nature of spatial variables such as the atomic position x. Each state can be detuned in energy by δ_j from Raman resonance, giving the following contribution to the Hamiltonian:

$$\hat{U} = \sum_{j=0}^{N-1} \delta_j |j\rangle\langle j|. \tag{2}$$

Finally, including the kinetic energy yields the full Hamiltonian,

$$\hat{H} = \frac{p^2}{2m} + \hat{V}(x) + \hat{U}, \tag{3}$$

where $p = -i\partial_x$ is the momentum operator, and in what follows we take $\hbar = 1$.

B. Dressed-state basis

Because the internal states $|j\rangle$ can be interpreted as sites in a synthetic dimension [18,19], it is convenient to adopt a synthetic "momentum" representation, giving a new basis of (position-independent) dressed states:

$$|\varepsilon_n\rangle = \frac{1}{\sqrt{N}} \sum_{j=0}^{N-1} |j\rangle e^{i2\pi nj/N}, \quad n = 0, 1, \ldots, N-1. \tag{4}$$

As above, we periodically label states implying $|\varepsilon_{n+N}\rangle = |\varepsilon_n\rangle$.

The light-matter-coupling operator [Eq. (1)] can be represented in the basis of dressed states as

$$\hat{V}(x) = \sum_l \hat{V}_l(x), \tag{5}$$

with terms

$$\hat{V}_l(x) = -\tilde{\Omega}_l \sum_{n=0}^{N-1} e^{i[2\pi(n+l)/N - 2k_R x]} |\varepsilon_n\rangle\langle\varepsilon_{n+l}| + \text{H.c.} \tag{6}$$

resulting from the lth Fourier component of the transition amplitudes

$$\tilde{\Omega}_l = \frac{1}{N}\sum_{j=0}^{N-1} \Omega_j e^{i2\pi l j/N}. \tag{7}$$

C. Dressed-state potential $V_0(x)$

We now consider the situation where the $l = 0$ Fourier component is dominant, so

$$\tilde{\Omega}_0 \gg \tilde{\Omega}_l, \quad l \neq 0. \tag{8}$$

The component

$$\Omega \equiv \tilde{\Omega}_0 = \frac{1}{N}\sum_{j=0}^{N-1} \Omega_j \tag{9}$$

is the average of the Rabi frequencies Ω_j. The corresponding contribution to $\hat{V}(x)$ is diagonal in the basis of dressed states $|\varepsilon_n\rangle$, giving

$$\hat{V}_0(x) = \sum_{n=0}^{N-1} \varepsilon_n(x) |\varepsilon_n\rangle\langle\varepsilon_n|, \tag{10}$$

where each

$$\varepsilon_n(x) = -2\Omega\cos(2k_R x - 2\pi n/N) \tag{11}$$

is a sinusoidal potential for atoms moving in $|\varepsilon_n\rangle$. The potentials $\varepsilon_{n\pm1}(x)$ for the neighboring dressed states $|\varepsilon_{n+1}\rangle$ and $|\varepsilon_{n-1}\rangle$ are each spatially shifted from $\varepsilon_n(x)$ by a distance $a = a_0/N$, giving a new unit cell that is N times smaller than the $a_0 = \lambda/2$ period of a conventional optical lattice. The dashed curves in Fig. 1(b) illustrate the lattice potentials $\varepsilon_n(x)$ for the case of three internal states ($N = 3$).

D. Coupling between dressed states

1. Coupling between dressed states via laser coupling

The Fourier components $\tilde{\Omega}_l$, with $l \neq 0$, induce tunable couplings $V_l(x)$ [Eq. (6)] between atoms in dressed states $|\varepsilon_{n+l}\rangle$ and $|\varepsilon_n\rangle$; the corresponding potential minima are separated by a distance la_0/N. The total contribution of these components is

$$\hat{V}'(x) = \sum_{l\neq0} \hat{V}_l(x). \tag{12}$$

Since each $\tilde{\Omega}_l$ is a discrete Fourier transform of the coupling matrix element Ω_j, changing its j dependence can generate a range of tunneling amplitudes $\tilde{\Omega}_l$ that can vary from short to long range. In the following we consider a uniform atom-light coupling $\Omega_j = \Omega$, and thus $\hat{V}(x) = \hat{V}_0(x)$, and concentrate on the effects of the detunings to be considered next.

2. Coupling between dressed states via detuning

The dressed states are also coupled via inhomogeneous (j-dependent) detunings δ_j. In the dressed-state basis the detuning operator (2) is

$$\hat{U} = \sum_{n=0}^{N-1}\sum_l U_l |\varepsilon_n\rangle\langle\varepsilon_{n+l}|, \tag{13}$$

where

$$U_l = \frac{1}{N}\sum_{j=0}^{N-1} \delta_j \exp\left(i\frac{2\pi l j}{N}\right) \tag{14}$$

describes coupling between dressed states $|\varepsilon_n\rangle$ and $|\varepsilon_{n+l}\rangle$ separated by l. The $l = 0$ term provides a uniform energy offset and will be omitted.

Similar to the case of inhomogeneous Rabi frequencies, the coupling matrix element U_l between dressed states $|\varepsilon_n\rangle$ and $|\varepsilon_{n+l}\rangle$ is a discrete Fourier transform of the detunings δ_j. Therefore, U_l can achieve a desired long-range structure on demand with the proper choice of the j dependence of δ_j.

It is useful to represent Eq. (3) for the full Hamiltonian as

$$\hat{H} = \hat{H}_0 + \hat{U}, \tag{15}$$

where the zeroth-order Hamiltonian

$$\hat{H}_0 = \frac{p^2}{2m} + \hat{V}_0(x) \tag{16}$$

consists of the kinetic-energy operator and the dressed-state potential $\hat{V}_0(x)$ defined by Eq. (10). In what follows we treat the detuning operator $\hat{U}$ as a perturbation which couples the dressed states.

E. Coupling dressed states with sinusoidal detuning

When the detuning

$$\delta_{j,l} = 2\delta\cos(2\pi l j/N - \varphi) \tag{17}$$

is a sinusoidal function of the internal state index j, the detuning operator (13) takes the simplified form

$$\hat{U}_l = \delta\sum_{n=0}^{N-1} |\varepsilon_n\rangle\langle\varepsilon_{n+l}| e^{i\varphi} + \text{H.c.}, \tag{18}$$

which couples dressed states $|\varepsilon_n\rangle$ and $|\varepsilon_{n+l}\rangle$ separated by l "sites" in a synthetic-dimension picture.

In what follows we consider detunings of the form

$$\delta_j = 2\sum_p \delta^{(p)}\cos(2\pi j/N - \varphi^{(p)}), \tag{19}$$

coupling only neighboring dressed states (i.e., $l = 1$, so we suppress the l index) with time-dependent phases $\varphi^{(p)} \equiv \varphi^{(p)}(t)$ and amplitudes $\delta^{(p)}$. In the remainder of this paper we focus on the specific case of three phases,

$$\varphi^{(p)}(t) = p\omega t + \gamma^{(p)} \quad (p = 0, \pm1), \tag{20}$$

with drive frequency ω and phase shifts $\gamma^{(p)}$. This leads to the detuning operator

$$\hat{U} = \sum_{n=0}^{N-1} F(t)|\varepsilon_n\rangle\langle\varepsilon_{n+1}| + \text{H.c.}, \tag{21}$$

where

$$F(t) = \sum_{p=0,\pm1} \delta^{(p)} e^{ip\omega t + i\gamma^{(p)}} \tag{22}$$

contains a time-independent component ($p = 0$) and a pair of components ($p = \pm 1$) with oscillatory exponents $\propto \exp(\pm i\omega t)$.

III. SYMMETRIES AND BLOCH STATES

A. Spatial shift by a_0 and Bloch solutions

The complete state vector of the system is

$$|\psi\rangle \equiv \int dx |\psi(x)\rangle \otimes |x\rangle, \tag{23}$$

where $|\psi(x)\rangle = \langle x|\psi\rangle$ is the state vector of the atomic internal states at the position x and $|x\rangle$ is the eigenvector of the position operator.

The atom-light-interaction operator $\hat{V}(x) = \hat{V}(x + a_0)$ in Eq. (1) has an obvious spatial periodicity of $a_0 = \pi/k_R$. As a result the Hamiltonian $\hat{H}$ commutes with the spatial displacement operator $T(\xi) \equiv \exp(ip_x\xi)$ for $\xi = a_0$, i.e., $[\hat{H}, T(a_0)] = 0$. The operators $\hat{H}$ and $T(a_0)$ can be simultaneously diagonalized, giving Bloch states

$$|\psi^{(k)}(x)\rangle = e^{ikx}|g^{(k)}(x)\rangle, \tag{24}$$

where

$$|g^{(k)}(x + a_0)\rangle = |g^{(k)}(x)\rangle \tag{25}$$

is the spatially periodic contribution and the crystal momentum k lies within the standard Brillouin zone (BZ) $-\pi/a_0 \leqslant k < \pi/a_0$. In the next section we identify an additional symmetry that reduces the unit cell to $a = a_0/N$.

B. Spatial shift by a

In addition to being invariant with respect to a spatial translation of a_0, the Hamiltonian $\hat{H}$ commutes with a combined translation operator

$$\hat{S}(\xi) = \hat{Q}T(\xi) \tag{26}$$

when $\xi = a$. The operator $T(a)$ implements a spatial shift by a distance N times smaller than the original lattice constant a_0.

The shift is accompanied by a change in the atomic internal state described by

$$\hat{Q} = \sum_{j=0}^{N-1} |j\rangle\langle j|e^{ij2\pi/N} = \sum_{n=0}^{N-1} |\varepsilon_{n+1}\rangle\langle\varepsilon_n|. \tag{27}$$

This is the synthetic-dimension displacement operator for the dressed-state basis. The combined symmetry operator $\hat{S}(a)$ is closely related to the magnetic displacement operators that appear in the study of the Hofstadter model of charged particles in a square lattice [20–22].

Because the Hamiltonian $\hat{H}$ is invariant with respect to the combined shift $\hat{S}(a)$, the operators $\hat{H}$ and $\hat{S}(a)$ have a common set of eigenstates analogous to the Bloch states in Eq. (24), but with N times smaller periodicity $a = a_0/N$. Thus, the eigenvectors $|\psi^{(k)}(x)\rangle$ of $\hat{S}(a)$ have eigenvalues $\exp(ika)$ characterized by a crystal momentum k covering an N-fold enlarged BZ with $-N\pi/a_0 \leqslant k < N\pi/a_0$.

The periodic part of these states has the property

$$\hat{Q}|g^{(k)}(x + a)\rangle = |g^{(k)}(x)\rangle, \tag{28}$$

so that

$$|g^{(k)}(x)\rangle = \sum_{n=1}^{N} g^{(k)}(x + na)|\varepsilon_n\rangle, \tag{29}$$

with $g^{(k)}(x + Na) = g^{(k)}(x)$.

IV. TIGHT-BINDING APPROACH

A. Wannier functions

We begin by considering maximally localized Wannier states associated with each dressed-state potential $\varepsilon_n(x)$ in the zeroth-order Hamiltonian $\hat{H}_0$ given by Eq. (16). The Wannier functions $\chi^{(\alpha)}(x - ar)$ for the nth dressed state are localized around each local minimum of $\varepsilon_n(x)$ at $x/a = r = n + Nl$. The integer l defines a periodic array of lattice sites, and $\alpha = 0, 1, \ldots$ (or, equivalently, $\alpha = s, p, \ldots$) labels the different Bloch bands.

The abstract state vector

$$|r,\ \alpha\rangle = \int dx \chi^{(\alpha)}(x - ar)|\varepsilon_r\rangle \otimes\ |x\rangle, \tag{30}$$

corresponding to the Wannier function $\chi^{(\alpha)}(x - ar)$, includes the dressed state $|\varepsilon_r\rangle = |\varepsilon_{n+Nl}\rangle = |\varepsilon_n\rangle$. Figures 2(a) and 2(b) plot Wannier functions for the two lowest bands, and the colors denote the different dressed states.

In the Wannier basis, the combined shift operator becomes

$$\hat{S}(a) = \sum_{r,\,\alpha} |r + 1,\ \alpha\rangle\langle r,\ \alpha|, \tag{31}$$

and the zeroth-order Hamiltonian reduces to

$$\hat{H}_0 = \sum_{\alpha,r} [\epsilon^{(\alpha)}|r,\ \alpha\rangle\langle r,\ \alpha| + J^{(\alpha)}(|r,\ \alpha\rangle\langle r + N,\ \alpha| + \text{H.c.})]$$

in the tight-binding limit with only NN tunneling. Here $J^{(\alpha)}$ is a matrix element for tunneling between NN Wannier functions in the same internal state, and $\epsilon^{(\alpha)}$ is the on-site energy. The tight-binding approximation holds for the lowest two bands (the s and p bands corresponding to $\alpha = 0$ and 1) when $\Omega \gtrsim 4E_R$. The vanishing of long-range tunneling in these bands is plotted in Figs. 2(c) and 2(d).

Although each dressed state is subject to a lattice with period a_0, the spacing between neighboring Wannier functions is $a = a_0/N$. These adjacent functions are in different dressed states with $|\varepsilon_n\rangle$ and $|\varepsilon_{n\pm1}\rangle$. This spacing is N times smaller than the original lattice constant a_0. This provides a one-dimensional lattice [shown by the dashed curves in Fig. 1(b) for $N = 3$] with a periodicity $a = a_0/N$, in which

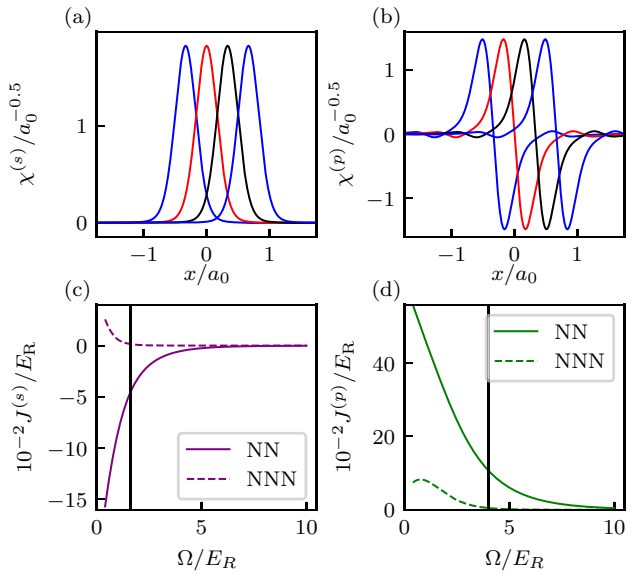

FIG. 2. Two-band model. (a) and (b) Wannier functions for the s band and p band, respectively, computed for $\Omega = 4E_R$, $\delta = 0E_R$, and $N = 3$. The colors correspond to Wannier states for each of the three dressed states. (c) and (d) Natural tunneling $J^{(\alpha)}$ dependence on Rabi frequency Ω for the s and p bands. The solid and dashed curves plot the nearest-neighbor (NN) and next-nearest-neighbor (NNN) tunneling. The black lines denote the threshold for the applicability of the tight-binding approximation: for $\alpha = s$ this threshold is $\Omega > 1.6E_R$, and for $\alpha = p$ it is $\Omega > 4.0E_R$.

the "natural tunneling" occurs between Wannier functions of the same dressed state separated by a_0.

As we will see in Sec. IV B, including the detuning operator $\hat{U}$ as a perturbation introduces tunneling between Wannier functions of different dressed states. Furthermore, as discussed in Sec. V, different Bloch bands—such as the s and p bands—can be coupled by making the detuning oscillatory in time.

B. Coupling between Wannier functions via detuning

The interaction operator $\hat{U}$ in Eq. (21) describes detuning-induced coupling between neighboring atomic internal dressed states $|\varepsilon_n\rangle$ and $|\varepsilon_{n+1}\rangle$. In the Wannier basis [defined in Eq. (30)], the leading-order contribution to $\hat{U}$ is

$$\hat{U} = F(t) \sum_{r,\alpha,\alpha'} |r,\,\alpha\rangle G_{\alpha,\alpha'} \langle r+1,\,\alpha'| + \text{H.c.}, \tag{32}$$

where

$$G_{\alpha,\alpha'} = \int_{-\infty}^{+\infty} \chi^{(\alpha)*}(x-a)\chi^{(\alpha')}(x)\,dx \tag{33}$$

is the overlap integral between the neighboring Wannier functions.

When the detuning is small compared to the energy difference between Bloch bands, $\hat{U}$ can be treated as a perturbation that induces transitions between spatially separated Wannier functions in different dressed states. For deep lattices (e.g., when $\Omega \gg E_R$), the matrix element of the direct tunneling $J^{(\alpha)}$ can be negligible in the lowest Bloch bands. This allows detuning-induced coupling between Wannier functions spaced by a (i.e., coupling neighboring dressed states) to become the dominant source of tunneling.

V. INTERBAND COUPLING VIA TIME-DEPENDENT DETUNING

The function $F(t)$ entering the detuning operator $\hat{U}(t)$ in Eqs. (21) and (32) contains a constant term $\delta^{(0)}$ and two Fourier components $\delta^{(\pm1)}\exp(\pm i\omega t)$. As we found in the last section, a constant detuning $\delta^{(0)}$ generates tunneling between neighboring Wannier functions in the same Bloch band, but for different dressed states. As we will see, the oscillatory terms $\propto \delta^{(\pm1)}\exp(\pm i\omega t)$ can resonantly couple Wannier functions in different Bloch bands and different dressed states $|\varepsilon_n\rangle$ and $|\varepsilon_{n+1}\rangle$.

The three-term form of $F(t)$ is in contrast to conventional periodic driving [23], where the tunneling matrix elements acquire phases such as $\propto \cos(\omega t)$. In that case, the tunneling elements are described by an infinite sum of Fourier components with amplitudes given by Bessel functions; this creates additional possibilities for unwanted coupling to higher Bloch bands.

A. Transition to the rotating frame

We focus on resonant driving where the energy difference between the ground (s) and first excited (p) bands is close to the driving frequency, i.e.,

$$|\epsilon^{(p)} - \epsilon^{(s)} - \omega| \ll \omega.$$

In this limit it is convenient to transform the tight-binding Hamiltonian into the rotating frame with the unitary transformation

$$\hat{S} = \exp\left(-i\omega t \sum_{\alpha,r} \alpha |r,\,\alpha\rangle\langle r,\,\alpha| \right). \tag{34}$$

The transformed Hamiltonian is

$$\tilde{H} = \tilde{H}_0 + \tilde{U}\,; \tag{35}$$

because $\hat{S}$ commutes with the zeroth-order Hamiltonian $\hat{H}_0$ but not $\tilde{U}$, we have

$$\tilde{H}_0 = \hat{H}_0 - i\hat{S}^\dagger \partial_t \hat{S}, \quad \tilde{U} = \hat{S}^\dagger \hat{U} \hat{S}, \tag{36}$$

where tildes mark transformed operators. In the Wannier basis the transformed operators are

$$\tilde{H}_0 = \sum_{\alpha,r} [\tilde{\epsilon}^{(\alpha)} |r,\,\alpha\rangle\langle r,\,\alpha| + J^{(\alpha)}(|r,\,\alpha\rangle\langle r+N,\,\alpha| + \text{H.c.})]$$

and

$$\tilde{U} = \sum_{\alpha,\alpha',r} [G_{\alpha,\alpha'} F(t) e^{i(\alpha'-\alpha)\omega t} |r,\,\alpha\rangle\langle r+1,\,\alpha'| + \text{H.c.}],$$

where

$$\tilde{\epsilon}^{(\alpha)} = \epsilon^{(\alpha)} - \alpha\omega \tag{37}$$

are the shifted energies of the Bloch bands.

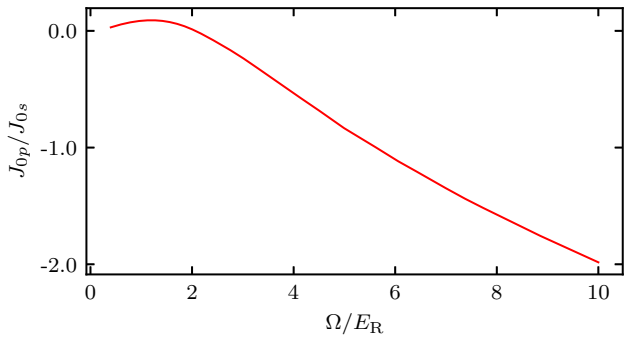

FIG. 3. Modulation-induced tunneling ratio J_{0p}/J_{0s} calculated exactly, plotted as a function of Ω.

B. Rotating-wave approximation

We now make the rotating-wave approximation (RWA) by omitting the oscillating terms remaining in the transformed operator $\tilde{U}$. We express the RWA detuning operator as the sum

$$\tilde{U} = \tilde{U}_0 + \tilde{U}_1 + \tilde{U}_{-1} \tag{38}$$

over three terms,

$$\tilde{U}_0 = \sum_{\alpha,r} [G_{\alpha,\alpha}\delta^{(0)} e^{i\gamma^{(0)}} |r,\ \alpha\rangle\langle r+1,\ \alpha| + \text{H.c.}], \tag{39}$$

$$\tilde{U}_1 = \sum_{\alpha,r} [G_{\alpha,\alpha-1}\delta^{(1)} e^{i\gamma^{(1)}} |r,\ \alpha\rangle\langle r+1,\ \alpha-1| + \text{H.c.}], \tag{40}$$

$$\tilde{U}_{-1} = \sum_{\alpha,r} [G_{\alpha,\alpha+1}\delta^{(-1)} e^{i\gamma^{(-1)}} |r,\ \alpha\rangle\langle r+1,\ \alpha+1| + \text{H.c.}], \tag{41}$$

where each term results from the corresponding term in $F(t)$. The time-independent detuning $\delta^{(0)}$ leads to $\tilde{U}_0$, which, as discussed above, describes tunneling between neighboring Wannier functions in the same Bloch band α. On the other hand, $\tilde{U}_{\pm 1}$ describe tunneling between neighboring Wannier functions in consecutive Bloch bands, where a transition from α to $\alpha \pm 1$ is accompanied by moving from site r to $r-1$ (and vice versa). These two processes are independent, as they are separately controlled by the amplitudes of the oscillating detunings $\delta^{(1)}$ and $\delta^{(-1)}$. Additionally, changing the drive frequency ω alters the RWA energy offsets of the Bloch bands $\tilde{\epsilon}^{(\alpha)}$.

We now specialize to the case where only the two lowest bands (identified by $\alpha = s$ or p) are coupled, in which case the components of $\tilde{U}$ reduce to

$$\tilde{U}_0 = \sum_{\alpha=s,p} \sum_r J_{0,\alpha} e^{i\gamma^{(0)}} |r,\ \alpha\rangle\langle r+1,\ \alpha| + \text{H.c.},$$

$$\tilde{U}_1 = \sum_r J_1 e^{i\gamma^{(1)}} |r,\ p\rangle\langle r+1,\ s| + \text{H.c.},$$

$$\tilde{U}_{-1} = \sum_r J_{-1} e^{i\gamma^{(-1)}} |r,\ s\rangle\langle r+1,\ p| + \text{H.c.},$$

with constants

$$J_{0\alpha} = G_{\alpha,\alpha}\delta^{(0)}, \quad J_{\pm 1} = \pm G_{p,s}\delta^{(\pm 1)}, \quad G_{p,s} = -G_{s,p}.$$

We find that $G_{s,s}$ is strictly positive, while $G_{p,p}$ is negative for $\Omega \gtrsim 4E_{\mathrm{R}}$, as indicated by the ratio $J_{0p}/J_{0s} = G_{p,p}/G_{s,s}$ plotted in Fig. 3. We also note that for $\Omega \lesssim 4E_{\mathrm{R}}$ coupling to higher bands cannot be neglected.

Altogether, this realizes a pair of RM chains [vertical lines in Fig. 1(c)] coupled by the static detuning δ_0 [diagonal lines in Fig. 1(c)]. The resulting physics, going beyond that of the RM model, is the focus of the remainder of this paper.

C. Coupled Rice-Mele chains

Because the full RWA Hamiltonian commutes with the combined translation operator $\hat{S}(a)$ given by Eq. (31), the eigenstates $|k, \beta\rangle$ are labeled by crystal momentum k (covering the extended Brillouin zone $-\pi/a \leqslant k < \pi/a$) as well as a band index β. Because the periodic modulation couples the initial bands (labeled by α), the eigenstates take the form

$$|k, \beta\rangle = \sum_\alpha c^{(\beta)}_{\alpha,k} |k,\ \alpha\rangle \tag{42}$$

in terms of the eigenstates

$$|k,\ \alpha\rangle = \frac{1}{L^{1/2}} \sum_r |r,\ \alpha\rangle e^{ikra}$$

of $\tilde{H}_0$ for a system L sites in extent.

When we consider only the two lowest bands, i.e., $\alpha \in \{s,\ p\}$, Eq. (42) reduces to

$$|k, \beta\rangle = c^{(\beta)}_{s,k} |k,\ s\rangle + c^{(\beta)}_{p,k} |k,\ p\rangle, \tag{43}$$

with $\beta = \pm$. Therefore, the eigenvalue equation $\tilde{H}|k, \beta\rangle = E_{k,\beta}|k, \beta\rangle$ can be expressed as a 2×2 matrix equation:

$$\tilde{H}_k \begin{pmatrix} c^{(\beta)}_{s,k} \\ c^{(\beta)}_{p,k} \end{pmatrix} = E_{k,\beta} \begin{pmatrix} c^{(\beta)}_{s,k} \\ c^{(\beta)}_{p,k} \end{pmatrix}, \tag{44}$$

where $\tilde{H}_k$ is the Hamiltonian matrix,

$$\tilde{H}_k = \begin{pmatrix} \Lambda_{s,k} & \Omega^*_k/2 \\ \Omega_k/2 & \Lambda_{p,k} \end{pmatrix}. \tag{45}$$

The off-diagonal matrix elements

$$\frac{\Omega_k}{2} = J_1 \exp[i(ka + \gamma^{(1)})] + J_{-1} \exp[-i(ka + \gamma^{(-1)})]$$

that couple the bands are due to the modulated detuning $\delta_{\pm 1}$. On the other hand, the diagonal matrix elements

$$\Lambda_{\alpha,k} = \tilde{\epsilon}^{(\alpha)} + 2J^{(\alpha)} \cos(kNa) + 2J_{0,\alpha} \cos(ka + \gamma^{(0)})$$

are due to the static detuning δ_0 and the natural tunneling $J^{(\alpha)}$.

In what follows we fix the modulation phases to be $\gamma^{(\pm 1)} = 0$ and $\gamma^{(0)} = -\pi/2$ and define the energy shift and detuning as

$$\Lambda_k = \frac{\Lambda_{s,k} + \Lambda_{p,k}}{2}, \quad \Delta_k = \Lambda_{s,k} - \Lambda_{p,k}. \tag{46}$$

Subtracting the overall Λ_k energy shift gives

$$\tilde{H}_k = \frac{1}{2} \begin{pmatrix} \Delta_k & \Omega^*_k \\ \Omega_k & -\Delta_k \end{pmatrix}. \tag{47}$$

Here Δ_k and Ω_k are

$$\Delta_k = \tilde{\epsilon} + 2J \cos(kNa) + 2J_0 \sin(ka) \tag{48}$$

and

$$\frac{\Omega_k}{2} = J_1 e^{ika} + J_{-1} e^{-ika}, \tag{49}$$

with

$$\tilde{\epsilon} = \tilde{\epsilon}^{(s)} - \tilde{\epsilon}^{(p)}, \quad J = J^{(s)} - J^{(p)}, \qquad J_0 = J_{0,s} - J_{0,p}.$$

For most parameters $J_{0,s}$ and $J_{0,p} < 0$, so in what follows we take $J_0 \geqslant 0$.

The eigenenergies of $\tilde{H}_k$ are

$$E_{k,\pm} = \pm\sqrt{\Delta_k^2 + |\Omega_k|^2}, \tag{50}$$

and the corresponding eigenstates [24,25]

$$|k,-\rangle = \begin{pmatrix} e^{-i\phi}\sin(\theta/2) \\ -\cos(\theta/2) \end{pmatrix}, \quad |k,+\rangle = \begin{pmatrix} e^{-i\phi}\cos(\theta/2) \\ \sin(\theta/2) \end{pmatrix}$$

can be represented in terms of the angles θ and ϕ, given by

$$e^{i\phi} = \Omega_k/|\Omega_k|, \qquad \cos\theta = 2\Delta_k/\Omega_k. \tag{51}$$

VI. ADIABATIC PUMPING

Here we consider the response of the system when one or more parameters are changed adiabatically and periodically in time with period T, making the eigenstates $|k,\pm;t\rangle$ explicit functions of time. In what follows the time dependence will be implicitly assumed.

A. Berry connection

In general any state $|\psi(\mathbf{u})\rangle$ parameterized by a set of variables u_j can be characterized by the geometric vector potential (Berry connection)

$$A_j = i\langle\psi(\mathbf{u})|\partial_j|\psi(\mathbf{u})\rangle. \tag{52}$$

In the present case we consider the eigenstates $|k,\pm\rangle$ of $\tilde{H}_k$ (which can be unambiguously defined only in the absence of degeneracies), giving

$$A_j^{(\pm)} = \mp\sin^2(\theta/2)\partial_j\phi, \tag{53}$$

with the parameters $u_j = (k,t)$. Because $|k,\pm\rangle$ is periodic in both k and t, $\mathbf{u}$ describe a torus embedded in a three-dimensional space. We correspondingly introduce a fictitious coordinate normal to the surface, giving

$$\mathbf{A}^{(\pm)} = (A_k^{(\pm)}, A_t^{(\pm)}, 0) = \mp\tfrac{1}{2}(1-\cos\theta)\nabla\phi. \tag{54}$$

The resulting geometric magnetic field (Berry curvature) is

$$\mathbf{B}^{(\pm)} = \nabla\times\mathbf{A}^{(\pm)} = (0,0,B) = \mp\tfrac{1}{2}\nabla\phi\times\nabla\cos\theta. \tag{55}$$

We will focus exclusively on the lower band of the coupled RM chain (consisting of a superposition of the ground and first excited bands of the physical lattice) in the remainder of this paper and therefore omit the $\pm$ superscript on $\mathbf{A}$ and $\mathbf{B}$ and take the lower sign in Eq. (55).

B. Chern number and Zak phase

We now consider the properties of this system when Hamiltonian parameters $\mathbf{u}(t)$ cyclically follow a closed path in parameter space. It is convenient (although not strictly necessary) to assume that this process is time periodic with period T. In this case and for a filled Bloch band, the system undergoes quantized pumping [2,25] described by an integer

$$C = \int_0^T \frac{dt}{2\pi}\int_{-\pi/a}^{\pi/a} dk B_z, \tag{56}$$

quantifying the per-cycle spatial displacement in units of the reduced lattice period a.

It is convenient to evaluate this integral using Stokes's formula to replace the planar integral in Eq. (56) with a line integral. The contribution by the boundary integration [Fig. (4)] vanishes because the vector potential $\mathbf{A}$ has periodicity $2\pi/a$ with respect to k and periodicity T with respect to t. Because the Stokes integration contour must avoid the singular points of $\mathbf{A}$, applying Stokes's formula to Eq. (56) with Eq. (54) for $\mathbf{A}$ yields

$$C = -\frac{1}{4\pi}\sum_{\text{sing}}\oint(1-\cos\theta)\nabla\phi\cdot d\boldsymbol{\ell}. \tag{57}$$

The sum runs over the singular points in $\mathbf{A}$ and the integration, around these points is counterclockwise; the overall minus sign results from the clockwise orientation of the original trajectories encircling the singular points, and the differential line element is $I\boldsymbol{\ell} = (Vk, ct, 0)$.

Adiabatic pumping can also be described by the Zak phase [26],

$$\gamma_{\text{Zak}} = \int_{-\pi/a}^{\pi/a} dk\, A_k. \tag{58}$$

In general, $a\gamma_{\text{Zak}}/(2\pi)$ gives the displacement of each Wannier function's mean position from an initial point (the selection of the initial position is arbitrary, and its selection behaves like a gauge-fixing condition). Therefore, changing the Zak phase by 2π leads to an overall spatial translation by the reduced lattice constant a: quantized pumping.

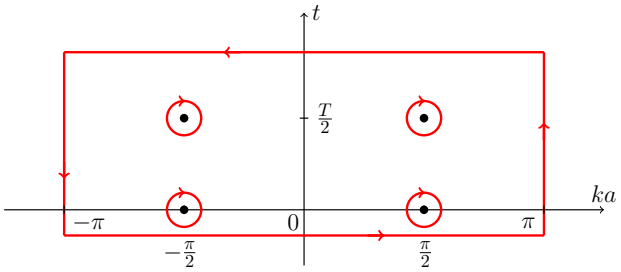

FIG. 4. Contours of integration. Due to the periodicity of the vector potential the boundary integration vanishes. Thus, the integral is fully defined by the small integrals around the excluded singular points in $\mathbf{A}$ given by Eq. (60).

C. Modulation schemes

Here we describe two specific adiabatic modulation schemes leading to topological charge pumping in the lowest band of the coupled RM chain. Both of these schemes involve modulations of $J_{\pm1}$. The first, which we call the "ϵ scheme," in addition modulates $\tilde{\epsilon}$, and the second, called the "J_0 scheme," instead adds modulation to J_0.

To achieve quantized adiabatic pumping, one must satisfy the following conditions. First, the periodicity of modulation T should be much larger than the s-p driving period, $T \gg 2\pi/\omega$. The second requirement is $T\,\Delta E_{\pm} \gg 1$, where $\Delta E_{\pm} = \min(E_{k,+} - E_{k,-})$ is the minimum band gap of the coupled RM chains during the pumping period. Note also that the temporal dependence of interchain and intrachain couplings (J_0 and $J_{\pm 1}$) is obtained by modulating the detunings δ_j of the two-photon Raman couplings. On the other hand, the time dependence of the on-site energy difference $\tilde{\epsilon}$ is controlled by modulating the s-p driving frequency ω.

We begin by considering the implications of modulating $J_{\pm 1}$ for the computation of the Chern number via Eq. (57). The singular points appearing in this expression occur when $\Omega_k = |\Omega_k| e^{i\phi} = 0$ and thus are located at $J_1 = J_{-1}$ and $ka = \pm\pi/2$.

Let us assume that the $s \to p$ tunneling elements J_1 and J_{-1} are modulated with opposite phases

$$J_{\pm 1} = \bar{J} \pm J_{\mathrm{R}} \sin(2\pi t/T), \tag{59}$$

where $J_{\mathrm{R}} \geqslant 0$. In this case, the only time-dependent reduced parameter in Eq. (47) is

$$\Omega_k = 4J\cos(ka) + i4J_{\mathrm{R}} \sin(2\pi t/T)\sin(ka).$$

The function Ω_k is zero at four points shown in Fig. 4 corresponding to the four possible combinations of

$$ka = \pm\pi/2, \quad t = jT/2, \quad j = 0, 1. \tag{60}$$

Integrating the phase gradient around each of these singular points yields

$$C = \frac{1}{2}\sum_{\pm}\sum_{j=0}^{1}(-1)^j[\mathrm{sgn}(\Delta_{\pm,j}) - 1] \tag{61}$$

via Eq. (57), where $\mathrm{sgn}(\cdot)$ is the sign function and

$$\Delta_{\pm,j} = \tilde{\epsilon} \pm 2J_0 \tag{62}$$

is the detuning Δ_k given by Eq. (48) at $ka = \pm\pi/2$ for $t = jT/2$.

In writing Eq. (62) we omitted the second term in Eq. (48), which is equal to zero for odd values of N. However, for even N it provides a small level shift which can be included in the detuning $\tilde{\epsilon}$.

1. ϵ modulation scheme

Here we consider the impact of additionally modulating the detuning

$$\tilde{\epsilon} = \bar{\epsilon} + \epsilon_{\mathrm{R}} \cos(2\pi t/T) \tag{63}$$

around a central value $\bar{\epsilon}$ with extent $\epsilon_{\mathrm{R}} \geqslant 0$. For $t = jT/2$, Eq. (62) reduces to

$$\Delta_{\pm,j} = \bar{\epsilon} + \epsilon_{\mathrm{R}}(-1)^j \pm 2J_0. \tag{64}$$

The red points in Fig. 5(a) mark the singular points in the $\tilde{\epsilon} - (J_1 - J_{-1})$ plane, and the circles show parametric trajectories in this plane.

As shown by the solid circle, both singular points are enclosed when

$$|\epsilon_{\mathrm{R}}| > |\bar{\epsilon} \pm 2J_0|. \tag{65}$$

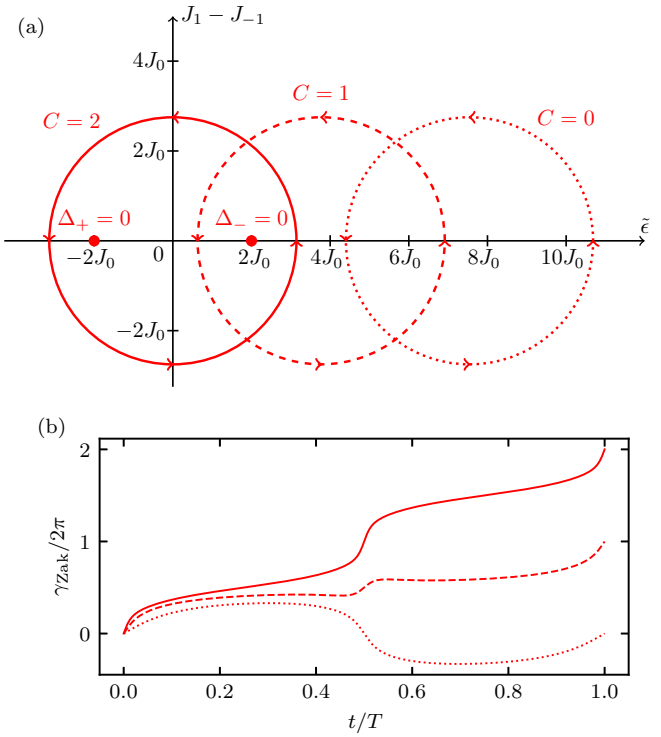

FIG. 5. Adiabatic pumping in the ϵ scheme. (a) The three circles show the cases when both critical points $(\pm 2J_0, 0)$ are encircled (solid), one of them is encircled (dashed), and neither is encircled (dotted). (b) Zak phase γ_{Zak} dependence on time t for the three aforementioned trajectories.

In this case, $\Delta_{\pm,j}$ alternates sign for even and odd values of j [because $\mathrm{sgn}(\Delta_{\pm,j}) = (-1)^j$], so Eq. (61) gives $C = 2$. Thus, one arrives at the adiabatic pumping displacement of $2a$ per pump cycle (like for uncoupled RM chains).

On the other hand, when only one of the conditions in Eq. (65) holds, just one point $(\pm 2J_0, 0)$ is encircled by the evolution curve [dashed circle in Fig. 5(a)], and $C = 1$. This leads to adiabatic pumping of a per cycle, a scenario which is not possible for uncoupled RM chains.

Finally, when neither condition holds, both points $(\pm 2J_0, 0)$ are outside the evolution curve [dotted circle in Fig. 5(a)], yielding the topologically trivial case with $C = 0$. Figure 5(b) shows the changes in the Zak phase for the three trajectories in Fig. 5(a), illustrating that the adiabatic pumping indeed takes place in units of $2a$, a, and 0 for these three cases.

2. J_0 modulation scheme

Last, we consider modulating

$$J_0 = \bar{J}_0 + J_{0,\mathrm{R}} \cos(2\pi t/T), \quad J_{0,\mathrm{R}} > 0, \tag{66}$$

rather than $\tilde{\epsilon}$. Using Eq. (62), we arrive at the detuning

$$\Delta_{\pm,j} = \tilde{\epsilon} \pm 2[\bar{J}_0 + J_{0,\mathrm{R}}(-1)^j], \tag{67}$$

where $\tilde{\epsilon}$ is taken to be constant and, without loss of generality, positive.

The red points in Fig. 6(a) denote singular points in the J_0-$(J_1 - J_{-1})$ plane, and like above, the circles plot different illustrative trajectories in this plane. As shown by the solid

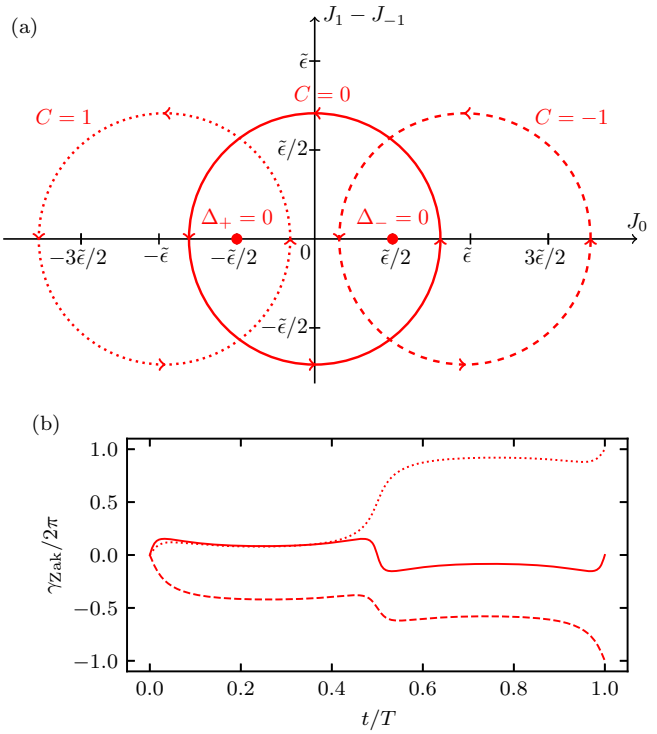

FIG. 6. Adiabatic pumping in the J_0 scheme. (a) Adiabatic pumping via modulation of $J_{\pm 1}$ and J_0 when both critical points $(\pm\tilde{\epsilon}/2, 0)$ are encircled (solid circle), the right point is encircled (dashed circle), and the left point is encircled (dotted circle). (b) Zak phase γ_{Zak} dependence on time t for the three aforementioned trajectories.

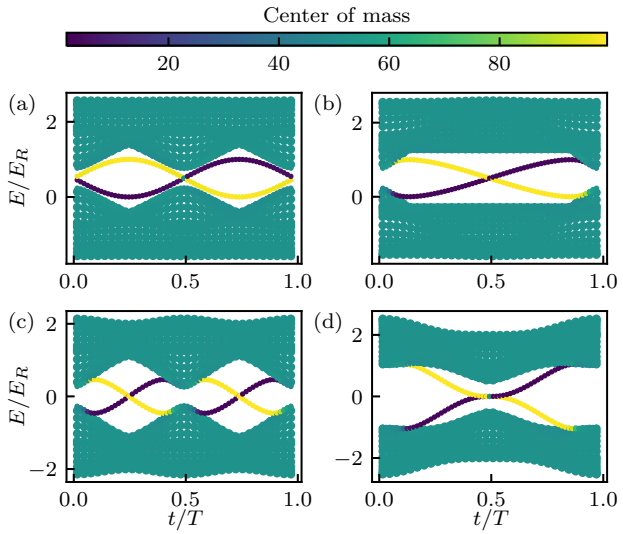

FIG. 7. Energy spectrum of finite coupled RM chains with $L = 100$ sites on each branch during the adiabatic pumping cycle. Color indicates the center-of-mass position of the instantaneous eigenstates. (a) and (b) correspond to the J_0 modulation scheme, while (c) and (d) correspond to the ϵ scheme. (a) and (c) show the case with both special points encircled, while (b) and (d) show the case with only one point.

circle, both singular points are enclosed when

$$|J_{0,\mathrm{R}}| > \left|\frac{\tilde{\epsilon}}{2} \pm \bar{J}_0\right|. \tag{68}$$

In this case, the detuning alternates for even versus odd j, so Eq. (61) sums to zero, giving Chern number $C = 0$ and no adiabatic pumping. On the other hand, when either condition in Eq. (68) holds, the point at $(\pm\tilde{\epsilon}/2, 0)$ is encircled [the dotted and dashed circles in Fig. 6(a)], giving $C = -1$ or $C = 1$, respectively. In these cases, adiabatic pumping gives a displacement of a single lattice constant a (to the right or to the left), once again, a scenario that is impossible for an uncoupled RM chain. Last, when neither condition holds, no singular point is encircled, and the system is again topologically trivial with $C = 0$.

Figure 6(b) shows the Zak phase for the three trajectories in Fig. 6(a), illustrating that the adiabatic pumping indeed yields displacement by 0 or $\pm a$. We also evaluated the Wannier-function centers by explicitly integrating the time-dependent Schrodinger equation and found them to be in exact agreement with the displacements predicted by the Zak phase. Changes in the Zak phase and energy gaps are presented in the Appendix.

VII. EDGE STATES

The bulk-edge correspondence links the properties of bounded and unbounded topological systems [27–29]. This correspondence indicates that finite systems will acquire edge modes—residing in the bulk energy gap—and that the number of such modes will be equal to the infinite-system topological invariant. We use this as an additional probe for the topology of the coupled RM model and turn our attention to a finite coupled RM chain with hard edges.

In Fig. 7, we plot the energy spectrum of eigenstates (colored according to center-of-mass position) calculated for the ϵ and J_0 modulation schemes and for two different paths. Exponentially localized edge states appear in the band-gap region, signaled by yellow and blue curves connecting bulk bands. When these states become degenerate, the system obeys a chiral symmetry, making the static system Zak phase a robust topological invariant. In this case these the degenerate states are the edge states predicted by the bulk-edge correspondence.

The movement of the edge state between bands during a pump cycle marks the transport of mass from one side of the system to the other. The first path encloses both special points, while the other encloses only one. The exact trajectories are depicted in Fig. 5(a) (solid and dashed curves) for the ϵ modulation scheme and Fig. 6(a) (solid and dotted curves) for the J_0 scheme.

We find a strict adherence to the bulk-edge correspondence: The number of edge states on each side of the system that flow from one band to another during each pump cycle is equal to the Chern number calculated in the previous section. Although Figs. 7(b) and 7(d) qualitatively resemble the edge-state flow of the conventional Rice-Mele model [30], the per-cycle displacement is reduced by half. Special attention should be given to Fig. 7(a), which shows edge states shifting in energy between the bands but never entering the bulk band and therefore not contributing to charge pumping. This further reinforces our conclusion that the coupled RM chain

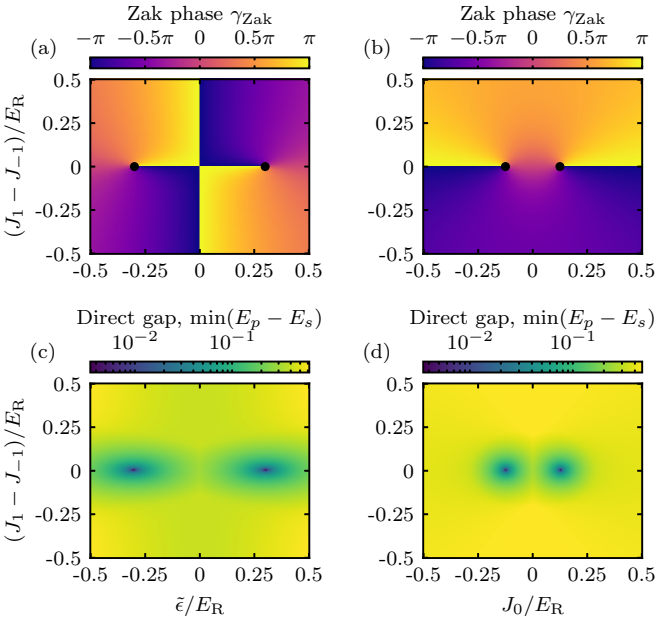

FIG. 8. Parameter regimes. (a) and (b) Zak phase γ_{Zak}. (c) and (d) Direct energy gap $\min(E_p - E_s)$. (a) and (c) correspond to the ϵ scheme, while (b) and (d) correspond to the J_0 scheme. All plots are calculated for $J_{\mathrm{avg}} = 0.1E_{\mathrm{R}}$.

described in this work is inherently different and cannot be explained by the superposition of two uncoupled RM chains.

VIII. CONCLUSION AND OUTLOOK

We described a lattice created by sequentially coupling internal atomic states using two-photon Raman transitions; this resulted in independent adiabatic potentials for each of the N dressed states. We showed that introducing a static detuning couples together these adiabatic potentials into a single lattice with $\lambda/(2N)$ periodicity.

We then studied the effects of time-modulated detuning to introduce effective tunneling matrix elements coupling the s and p bands, leading to a subwavelength optical lattice. We interpreted this lattice as a pair of coupled RM chains described by a highly tunable two-leg ladder Hamiltonian with unique topological properties. We showed that this lattice exhibits unusual behavior in terms of topological pumping and edge states. In the former case we showed that the added interchain tunneling enables simple pumping trajectories giving per-cycle displacements of zero, one, or two unit cells, in contrast to the zero- or two-cell displacements allowed for uncoupled RM chains.

The present work suggests several directions for future inquiry. Here we focused only on nearest-neighbor detuning-induced tunneling; however, more complicated lattice topologies can be created by exploiting the long-range tunneling induced by detuning in Eq. (19). Even without coupling s and p bands this may enable new ways to engineer locally flat bands [31,32] where interaction effects can dominate.

In addition, lattices in two and three dimensions can be created by going to larger spin systems; going beyond the suggestions in Refs. [3,4] for creating conventional lattices, it is also possible to use coupled internal states to define a discretized torus rather than a closed loop in the space of coupled internal states.

The generic scheme described here is not limited to crystalline order. For example, a bichromatic subwavelength lattice can be created by adding Raman coupling with a wave number incommensurate with k_{R}. This would open up possibilities to study localization phenomena with tunable single-particle mobility edges [33,34]

Topological charge pumps obtain their robustness by fully filling a collection of Bloch bands. One could investigate the more general case of geometric charge pumping [35] that lifts this constraint. Given the flexibility of this lattice, one might engineer the local Berry connection $A_k(k)$ to enhance the performance of geometric charge pumps, either for improved robustness or even for increased per-cycle displacement.

ACKNOWLEDGMENTS

The authors thank T. Andrijauskas and E. Gvozdiovas for productive discussions and A. M. Piñeiro and M. Zhao for carefully reading the manuscript. The authors acknowledge support from the Research Council of Lithuania (Grant No. S-MIP-20-36). This work was partially supported by the National Institute of Standards and Technology, the National Science Foundation through the Quantum Leap Challenge Institute for Robust Quantum Simulation (Grant No. OMA-2120757), and the Air Force Office of Scientific Research via the RAPSYDY in Q Multidisciplinary University Research Initiative (Grant No. FA9550-22-1-0339).

APPENDIX: ZAK PHASE AND ENERGY GAPS

As shown in Figs. 8(a) and 8(b), to advance the Zak phase by $+2\pi$, one has to encircle either of the singular points in the same direction (counterclockwise) for the ϵ scheme but in opposite directions for the J_0 scheme (counterclockwise for $\Delta_+ = 0$ and clockwise for $\Delta_- = 0$). Thus, both critical points have the same topological charge for the ϵ case but opposite charges in the J_0 case.

As one approaches the critical points in parameter space, the direct gaps grow smaller and smaller [see Figs. 8(c) and 8(d)]. Thus, if the encirclement radius is small, the adiabatic pumping period T must be larger to satisfy the adiabaticity condition.

[1] M. J. Rice and E. J. Mele, Phys. Rev. Lett. **49**, 1455 (1982).

[2] D. J. Thouless, Phys. Rev. B **27**, 6083 (1983).

[3] R. P. Anderson, D. Trypogeorgos, A. Valdés-Curiel, Q.-Y. Liang, J. Tao, M. Zhao, T. Andrijauskas, G. Juzeliūnas, and I. B. Spielman, Phys. Rev. Res. **2**, 013149 (2020).

[4] C.-H. Li, Y. Yan, S.-W. Feng, S. Choudhury, D. B. Blasing, Q. Zhou, and Y. P. Chen, PRX Quantum **3**, 010316 (2022).

[5] G. Ritt, C. Geckeler, T. Salger, G. Cennini, and M. Weitz, Phys. Rev. A **74**, 063622 (2006).

[6] T. Salger, G. Ritt, C. Geckeler, S. Kling, and M. Weitz, Phys. Rev. A **79**, 011605(R) (2009).

[7] N. Lundblad, P. J. Lee, I. B. Spielman, B. L. Brown, W. D. Phillips, and J. V. Porto, Phys. Rev. Lett. **100**, 150401 (2008).

[8] N. Lundblad, S. Ansari, Y. Guo, and E. Moan, Phys. Rev. A **90**, 053612 (2014).

[9] Y. Wang, S. Subhankar, P. Bienias, M. Łącki, T.-C. Tsui, M. A. Baranov, A. V. Gorshkov, P. Zoller, J. V. Porto, and S. L. Rolston, Phys. Rev. Lett. **120**, 083601 (2018).

[10] T.-C. Tsui, Y. Wang, S. Subhankar, J. V. Porto, and S. L. Rolston, Phys. Rev. A **101**, 041603(R) (2020).

[11] R. Dum and M. Olshanii, Phys. Rev. Lett. **76**, 1788 (1996).

[12] G. Juzeliūnas, J. Ruseckas, P. Öhberg, and M. Fleischhauer, Phys. Rev. A **73**, 025602 (2006).

[13] D. L. Campbell, G. Juzeliūnas, and I. B. Spielman, Phys. Rev. A **84**, 025602 (2011).

[14] F. Jendrzejewski, S. Eckel, T. G. Tiecke, G. Juzeliūnas, G. K. Campbell, L. Jiang, and A. V. Gorshkov, Phys. Rev. A **94**, 063422 (2016).

[15] M. Łącki, M. A. Baranov, H. Pichler, and P. Zoller, Phys. Rev. Lett. **117**, 233001 (2016).

[16] E. Gvozdiovas, P. Račkauskas, and G. Juzeliūnas, SciPost Phys. **11**, 100 (2021).

[17] E. Bertok, F. Heidrich-Meisner, and A. A. Aligia, Phys. Rev. B **106**, 045141 (2022).

[18] O. Boada, A. Celi, J. I. Latorre, and M. Lewenstein, Phys. Rev. Lett. **108**, 133001 (2012).

[19] A. Celi, P. Massignan, J. Ruseckas, N. Goldman, I. B. Spielman, G. Juzeliūnas, and M. Lewenstein, Phys. Rev. Lett. **112**, 043001 (2014).

[20] J. Zak, Phys. Rev. **134**, A1602 (1964).

[21] D. R. Hofstadter, Phys. Rev. B **14**, 2239 (1976).

[22] B. A. Bernevig, *Topological Insulators and Topological Superconductors* (Princeton University Press, Princeton, NJ, 2013).

[23] A. Eckardt, Rev. Mod. Phys. **89**, 011004 (2017).

[24] J. Dalibard, F. Gerbier, G. Juzeliūnas, and P. Öhberg, Rev. Mod. Phys. **83**, 1523 (2011).

[25] D. Xiao, M. C. Chang, and Q. Niu, Rev. Mod. Phys. **82**, 1959 (2010).

[26] J. Zak, Phys. Rev. Lett. **62**, 2747 (1989).

[27] Y. Hatsugai, Phys. Rev. Lett. **71**, 3697 (1993).

[28] B. I. Halperin, Phys. Rev. B **25**, 2185 (1982).

[29] K. Yatsugi, T. Yoshida, T. Mizoguchi, Y. Kuno, H. Iizuka, Y. Tadokoro, and Y. Hatsugai, Commun. Phys. **5**, 180 (2022).

[30] J. K. Asbóth, L. Oroszlány, and A. Pályi, *A Short Course on Topological Insulators* (Springer, Switzerland, Cham, 2016).

[31] K. Sun, Z. Gu, H. Katsura, and S. Das Sarma, Phys. Rev. Lett. **106**, 236803 (2011).

[32] E. J. Bergholtz and Z. Liu, Int. J. Mod. Phys. B **27**, 1330017 (2013).

[33] H. P. Lüschen, S. Scherg, T. Kohlert, M. Schreiber, P. Bordia, X. Li, S. Das Sarma, and I. Bloch, Phys. Rev. Lett. **120**, 160404 (2018).

[34] X. Li, X. Li, and S. Das Sarma, Phys. Rev. B **96**, 085119 (2017).

[35] H.-I. Lu, M. Schemmer, L. M. Aycock, D. Genkina, S. Sugawa, and I. B. Spielman, Phys. Rev. Lett. **116**, 200402 (2016).